Research Article

Photocatalytic degradation of chlorpyrifos and methylene blue using α-Bi_2O_3 nanoparticles fabricated by sol–gel method

Subhash Dharmraj Khairnar[1] · **Vinod Shankar Shrivastava**[1]

Abstract

Organic dyes and pesticides, i.e. methylene blue and chlorpyrifos are the most frequently used in the various fields in everyday life for the different purpose. The presence of organic dyes and pesticides within the aquatic environment causes serious problems to the both types ecosystems. The aim of this study, to evaluate the photocatalytic degradation of methylene blue and chlorpyrifos in aqueous solution using α-Bi_2O_3 nanoparticles (NPs). The α-Bi_2O_3 NPs were successfully synthesized by sol–gel method and characterized by XRD, SEM, TEM, EDX and FTIR techniques. Moreover, the photocatalytic degradation of methylene blue and chlorpyrifos was investigated by optimizing the various parameters like pH, an initial concentration of the solution, irradiation time and photocatalyst dose, etc. The photocatalytic efficiency of α-Bi_2O_3 NPs was measured using a UV–visible double beam spectrophotometer. The results show that the α-Bi_2O_3 NPs have an average crystallite size of 32.47 nm with a highly rough and porous surface area. The optimized condition for the photocatalytic degradation was obtained at pH = 2 and pH = 5, the initial concentration of solution 10 mg/L and irradiation time 90 min for methylene blue and chlorpyrifos respectively. Besides this, the kinetics of photocatalytic degradation were investigated and the results indicate that the photocatalytic degradation of methylene blue and chlorpyrifos follows the pseudo-first order kinetics.

✉ Vinod Shankar Shrivastava, drvinodshrivastava1962@gmail.com; Subhash Dharmraj Khairnar, subhashkhairnar20@gmail.com | [1]Nano-Chemistry Research Laboratory, G. T. Patil College, Nandurbar, M.S 425412, India.

SN Applied Sciences (2019) 1:762 | https://doi.org/10.1007/s42452-019-0761-4

Received: 12 April 2019 / Accepted: 11 June 2019 / Published online: 21 June 2019

Graphic abstract

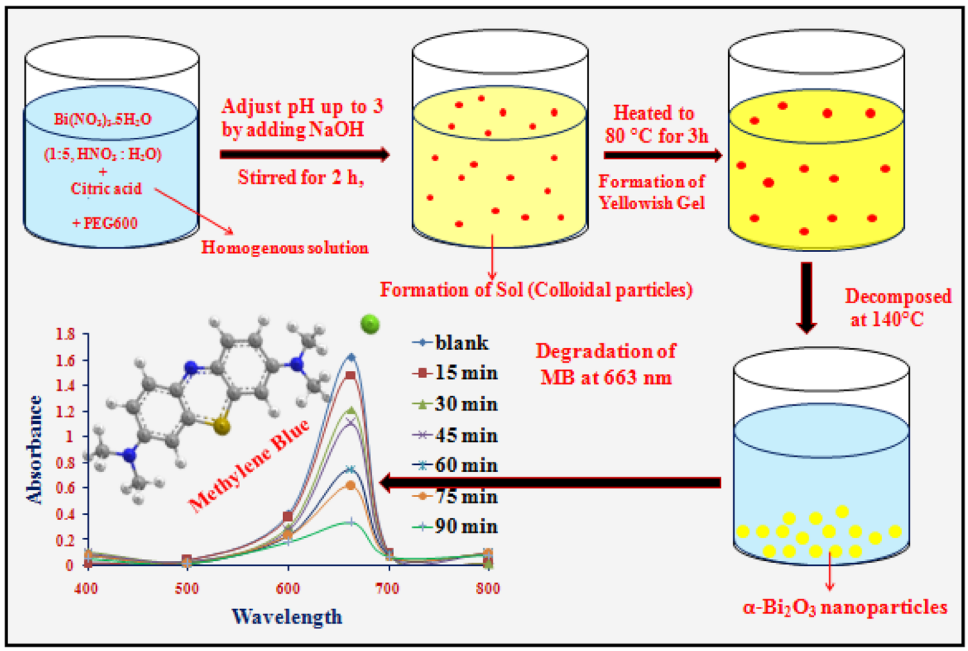

Keywords Chlorpyrifos · Organic pesticides · α-Bi_2O_3 · Pseudo first order · Methylene blue

1 Introduction

In India the majority of peoples totally rely on agricultural production because it is the main occupation of most of the Indian villagers. Agriculture is a standout amongst the most essential factors in the Indian economy and contributes 18% to the GDP. Which ensuring the nourishment, security for more than 1.37 billions of Indian populations with the diminishing cultivable land resource is a Herculean task. India is the second largest producer of agricultural products. India accounts for 7.39% of the total global agricultural output. In the process of accomplishing the target pesticides play an important role in Indian farming. Pesticides are the agrochemicals, one of the invaluable inputs in sustaining agricultural production as substantial food production is lost due to insect pests, plant pathogens, weeds, etc. However, since the green revolution (1966) has been begun in India, the application of these chemicals expanded in excess of multiple times and causing tremendous loss to the environment and human health. Internationally big effort is made to safe use of chemicals. In India nearly 65% of the workforce derives a livelihood from agriculture and are therefore exposed to chemical pesticides. The rampant use of pesticides has played havoc with living beings and the environment as these chemicals persists and seep into the environment for a long time because of more water solubility, tendency to adsorb to the soil (soil adsorption) and more half-life that tends to persist in the environment.

Chlorpyrifos, O,O-diethyl O-(3,5,6-trichloro-2-pyridyl) phosphorothioate [$C_9H_{11}Cl_3NO_3PS$] (CPS), is a well-known organophosphorothioate pesticide that is widely used in agricultural and nonagricultural fields [1]. The Indian government has restricted various chlorinated hydrocarbons pesticides such as Aldrin, DDT and Chlordane etc., and the use of CPS has increased as an alternate option [2]. Exposure to CPS and its metabolites has been related to a variety of nerve disorders in humans. CPS shows a wide spectrum of biological activity and is used to control a range of insects, pests as well as soil-dwelling grubs, rootworms, borers and subterranean termites. The contamination has been found up to about 24 km from the site of application. Symptoms of acute poisoning include headache, nausea, muscle twitching and convulsions and in some extreme cases even death. A human birth defects have also been associated with exposure to CPS and its products. It also affects the male reproductive system. CPS is toxic to a variety of beneficial arthropods, including bees, ladybird beetles and parasitic wasps. It kills fish at concentrations as low as a few parts per trillion [3–5]. Therefore, the degradation of CPS present in the environment has become a public concern.

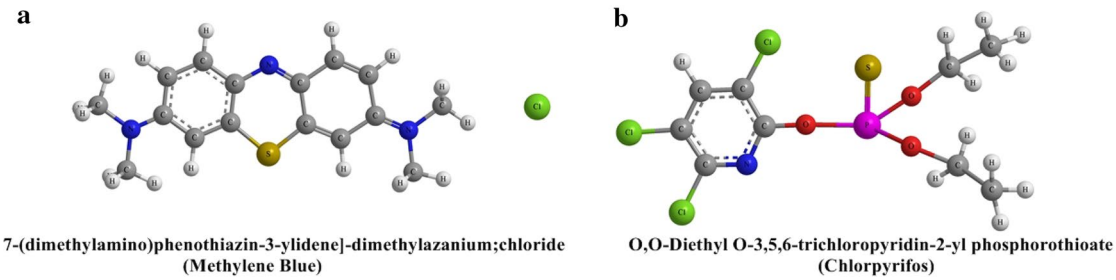

Fig. 1 3D structures of **a** methylene blue, **b** chlorpyrifos

Nanotechnology is imperative with regards to environmental remediation [6, 7]. Photocatalytic degradation has been proved to be a promising method for the treatment of wastewater contaminated with organic and inorganic pollutants. In recent years, advanced oxidation processes (AOPs) have been proposed as innovative water treatment technologies. The prominent feature of these AOPs is based on the in situ generations of active species (i.e., H_2O_2, $HO^{\cdot}$, $O2^{-\cdot}$, and O_3) for the mineralization of refractory organic compounds, water pathogens and disinfection by products [8–14]. Heterogeneous photocatalysis, which accelerating the photoreaction by a catalyst, an attractive and efficient method for the degradation of environmental pollutants or non-biodegradable toxics present in domestic sewage, industrial or agricultural effluents [15]. Among various semiconductors a p-type Bi_2O_3 heterogeneous semiconductor was considered as one of the most proficient photocatalysts and important in modern solid state because of its unique structures and physical characteristics like high refractive index, high oxygen-ion conductivity, dielectric permittivity and thermal stability, Bi_2O_3 is inert towards neutral water and possess band gap energy in the visible region (~ 2.9 eV) can oxidise water and produce highly reactive species for initiating oxidation reaction for degradation of pesticides and dyes [15, 16]. Pure Bi_2O_3 exists five polymorphisms: α-Bi_2O_3, β-Bi_2O_3, γ-Bi_2O_3, δ-Bi_2O_3, ε-Bi_2O_3 [17]. α-Bi_2O_3 transforms into δ-Bi_2O_3at 729 °C, upon cooling δ-Bi_2O_3 transfer into β-Bi_2O_3 at 650 °C [17, 18]. Among them, high-temperature δ-phase and the low-temperature α-phase are stable, whereas β-Bi_2O_3, γ-Bi_2O_3 and ε-Bi_2O_3 forms are metastable [17]. Among all phases the band gap of the low-temperature a phase is 2.8 eV and therefore found to be active in the visible region [19, 20].

Methylene blue (MB) is a severe pollutant since it is widely used as a colorant in various industries for the different purpose. It is harmful and carcinogenic to human beings [21, 22]. Therefore, it is necessary to remove such hazardous dyes and pesticides from natural water bodies. In this study, we first time report a study on the photocatalytic degradation of CPS and MB independently using α-Bi_2O_3 NPs fabricated by the sol–gel method.

2 Experimental

2.1 Materials and methods

All the chemicals used in the present study are of A.R.grade. Bismuth nitrate pentahydrated [$Bi(NO_3)_3{\cdot}5H_2O$], Citric acid, Polyethylene glycol 600 (PEG600), Sodium hydroxide (NaOH), Methylene blue and nitric acid were purchased from S. D. Fine Chemicals, Mumbai, India and Chlorpyrifos were purchased from local markets and used without any purification. The 3D structures of Methylene blue and chlorpyrifos are as shown in Fig. 1a, b.

2.2 Preparation of dye and pesticide solutions

The stock solution (100 mg/L) of MB and CPS was prepared using deionized water. The experimental solution of the desired concentration of MB and CPS (10, 15, and 20 mg/L) was prepared by further dilution of the stock solution with deionized water.

2.3 Synthesis of α-Bi_2O_3 nanoparticles

0.1 M of Bi $(NO_3)_3.5H_2O$ was dissolved in 100 ml of nitric acid solution (1:5, HNO_3: H_2O) and mixed with 2 gm of citric acid. In order to prevent agglomeration, a small amount of PEG600 was added as a surfactant. The pH of the solution was adjusting 3 by adding NaOH and the above solution was stirred for 2 h, then a sol formed. The sol solution was heated to 80 °C for 3 h to form a yellowish gel. This gel was decomposed at 140 °C in oven. The gel initially started to swell and filled the beaker producing a foamy precursor. This foam consists of homogeneous flakes of very small particle size.

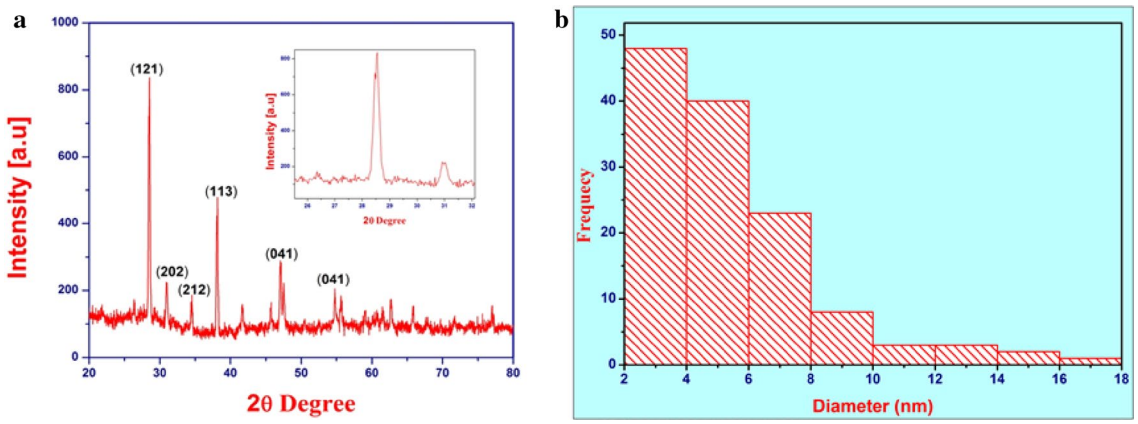

Fig. 2 **a** The XRD patterns of α-Bi_2O_3 NPs, **b** particle size distribution from SEM images of α-Bi_2O_3 NPs

2.4 Photocatalytic degradation experiments

The photocatalytic degradation of MB and CPS were carried out in a photocatalytic reactor (Photocatalytic reactor, Lelesil Innovative System, Mumbai) under the UV visible light irradiation with the help of 160 W mercury lamp (wavelength range 200–690 nm). The synthesized α-Bi_2O_3 NPs was added in 50 ml of an aqueous solution of MB and CPS. Then the solution is kept in the photocatalytic reactor with continuous stirring to ensure that the suspensions of the catalyst were uniform over the span of reaction. At regular intervals, adequate amount of sample solution was removed and centrifuged for 10 min to separate α-Bi_2O_3 NPs. After that the supernatant solution was analyzed with the help of UV–visible double beam spectrophotometer at the wavelength of absorbance maximum (for MB $\lambda_{max} = 663$ nm and CPS $\lambda_{max} = 308$ nm) to obtain the concentration of MB and CPS in solution. The percentage of degradation of dye has been calculated by using Eq. 1.

$$\%Degradation = \frac{(C_0 - C_t)}{C_0} \times 100 \quad (1)$$

where C_o is the initial concentration and C_t is the concentration after time t.

2.5 Characterizations

The synthesized α-Bi_2O_3 NPs was characterized by scanning electron microscopy (SEM Hitachi S-4800 Japan), Transmission electron microscopy (TEM), X-ray diffraction (XRD-Bruker D 8 Advance X-ray diffractometer Germany), electron dispersive X-ray spectroscopy (EDX-Bruker X Flash 5030), Fourier-transform infrared spectroscopy (Shimadzu FTIR-8400) techniques and the photocatalytic activity was performed by a UV–Vis spectrophotometer (Systronics 2203 India).

3 Results and discussion

3.1 X-ray diffraction analysis

The X-ray diffraction analysis of synthesized α-Bi_2O_3 NPs are as shows in Fig. 2a. The diffraction patterns of α-Bi_2O_3 were (121), (202), (212), (113), (041) and (241) reflection planes at 28.55, 30.92, 34.55, 38.15, 47.06, 54.77 and 55.64, 2θ position enlightening the monoclinic crystal structure of α-Bi_2O_3 in accordance with JCPDS card No. 00-041-1449, Confirming the phase purity of synthesized α-Bi_2O_3 NPS. The high intensity peak of (121), (113) and (041) peaks were suggested the better growth of α-Bi_2O_3 NPs. The inset of Fig. 2a shows the magnified image of a plane (121) at 28.55 2θ position. Figure 2b shows the particle size distribution obtained from SEM images. The results clearly indicated the synthesized α-Bi_2O_3 NPs have a particle size under the 20 nm and the maximum particle has a diameter in the range of 2–4 nm.

Table 1 shows the lattice parameters and the average crystallite size of α-Bi_2O_3 NPs, which were calculated from FWHM of XRD peaks at 28.55, 30.92, 34.55, 38.15, 47.06, 54.77 and 55.64, 2θ position using Scherer formula given in Eq. 2 [23].

$$D = \frac{0.94\lambda}{\beta \mathrm{Cos}\theta} \quad (2)$$

where D is the average crystalline size, λ is a wavelength in A^0, β is the FWHM in radian and θ is diffraction angle in degree. The average crystallite size of the α-Bi_2O_3 NPS were 32.47 nm.

3.2 UV–visible absorption spectra

The UV–visible absorption spectra of α-Bi_2O_3 NPs is as shown in Fig. 3. The absorption data further utilized to

Table 1 The lattice parameters of α-Bi_2O_3 NPs

Catalyst	Lattice parameters (A^0)			2θ Degree	(h k l) Planes	FWHM (β)	Crystallite size (nm)
	a	b	c				
Bi_2O_3	5.8510	8.1324	7.5321	28.55	121	0.24892	34.42
				30.92	202	0.34969	24.64
				34.55	212	0.22676	38.35
				Average crystalline size			32.47

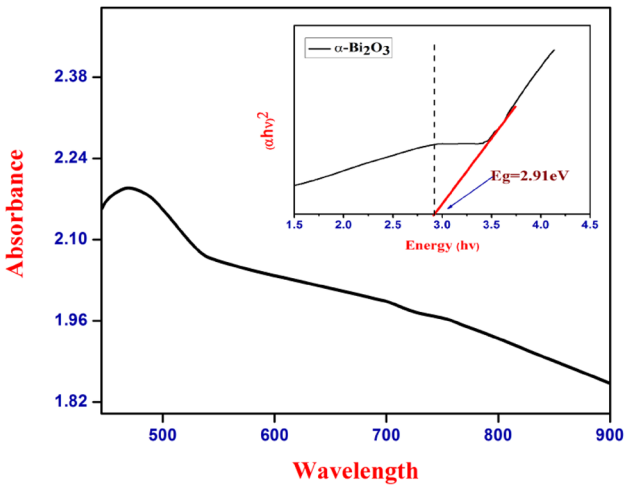

Fig. 3 UV–visible absorption spectra of α-Bi_2O_3 NPs and inset image is the Tauc's plot

calculate the band gap energy, obtained by plotting the graph between $(\alpha h\nu)^2$ Vs hν as shown in inset of Fig. 3. Where h, α and ν represent the Planck constant, absorption coefficient, and the incident light frequency respectively. Based on the Tauc's plot the direct band gap (E_g) of α-Bi_2O_3 Nps are 2.91 eV which shows the good agreement with previous literature [24] and indicating the high absorption of α-Bi_2O_3 Nps in the visible as well as in UV region.

3.3 Morphology

To achieve the information regarding the particle morphology, the synthesized α-Bi_2O_3 NPs were examined by scanning electron microscopy (SEM). The SEM results of α-Bi_2O_3NPs revealed a large number of small, interconnected spherical grains with a high rough and porous surface Fig. 4a, b. The nanoporous surface of α-Bi_2O_3 photocatalyst enables the electrolyte to permeate into the surface, react with photogenerated holes directly on the particle surface. So, the porous surface of the photocatalyst could potentially promote the charge transfer process [24, 25] and eventually enhance the photocatalytic efficiency. Also, a confirmation of morphology and crystallite size was carried out by Transmission electron microscopy (TEM) analysis. The TEM images of α-Bi_2O_3 NPs shows that

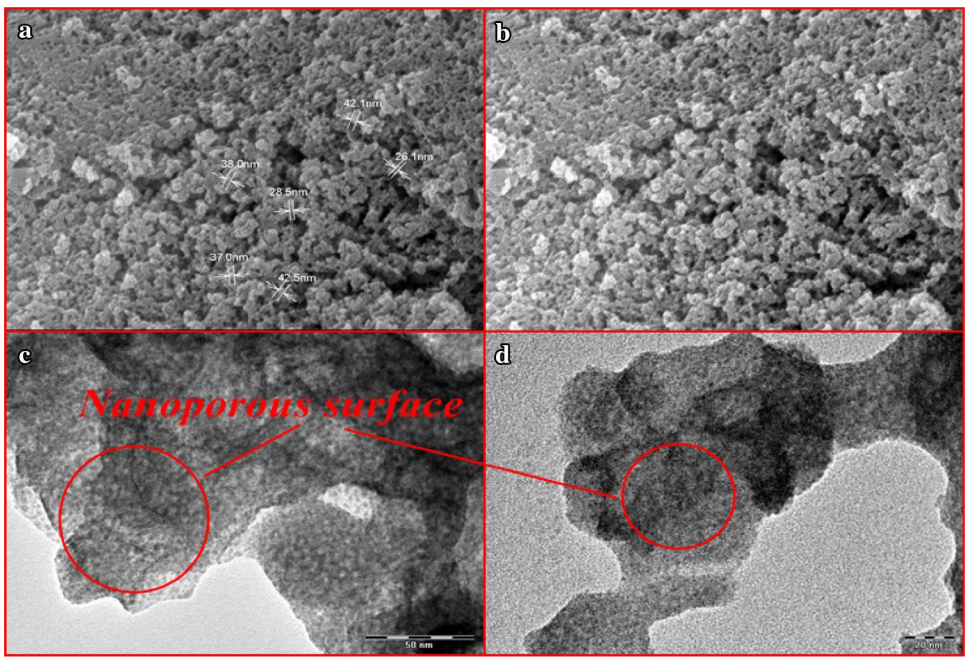

Fig. 4 **a**, **b** SEM images of α-Bi_2O_3 NPs, **c**, **d** TEM images of α-Bi_2O_3 NPs

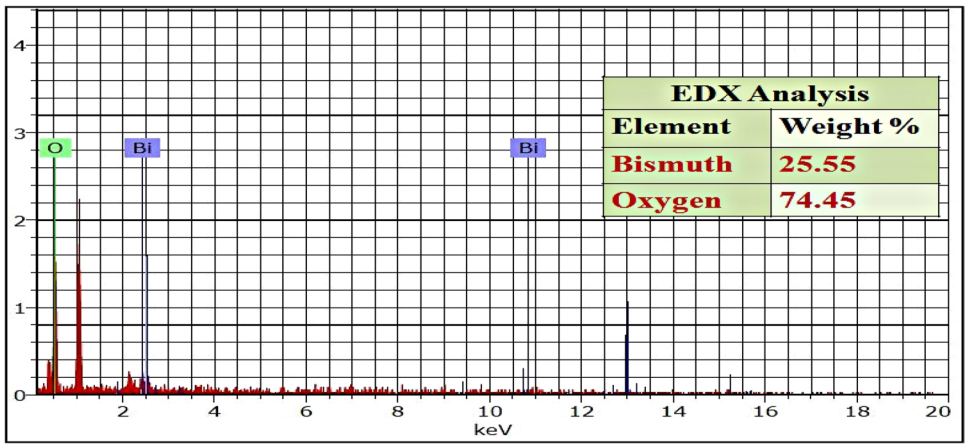

Fig. 5 Energy-depressive X-ray analysis of α-Bi_2O_3 NPs

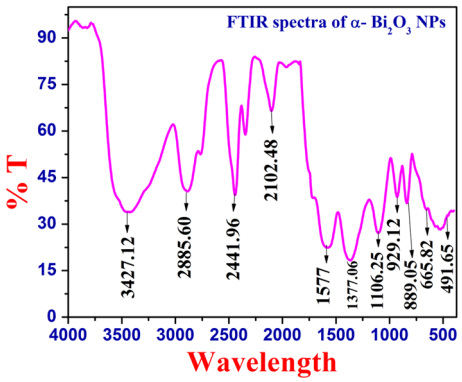

Fig. 6 FTIR spectra of α-Bi_2O_3 NPs

the α-Bi_2O_3 NPs were spherical grains with porous morphology and crystallite size in the range of 1–100 nm as shown in Fig. 4c, d.

3.4 Energy-depressive X-ray spectroscopy (EDS)

The formation of α-Bi_2O_3 NPs is also confirmed by EDX analysis and the results are shown in Fig. 5. The energy dispersive X-ray spectroscopy of a α-Bi_2O_3 indicate the sharp peaks of Bismuth and oxygen at 10.8 keV and 0.5 keV respectively, whereas the α-Bi_2O_3 consisted of 55% bismuth and 45% oxygen. No other impurity was detected in sample spectrum, which confirms the purity of the α-Bi_2O_3 NPs.

3.5 Functional group analysis (FTIR)

For the determination of functional group present in the synthesized NPS, Fourier-transform infrared spectroscopy (FTIR) analysis was carried out. Figure 6 shows the FT-IR spectra of α-Bi_2O_3 NPs. The absorption band at 3427 and 1577 cm^{-1} is due to the –OH stretching and bending vibrations [26]. The band at 1377 cm^{-1} is the characteristic peak of the interlayer nitrate. The absorption peak at 1106 cm^{-1} is due to the –OH group stretching vibration of the H_2O molecule in α-Bi_2O_3 lattice [27]. In general, metal oxide shows the absorption band below 1000 cm^{-1} therefore, the absorption band at 889 and 665 cm^{-1} is typical bismuth oxygen bond stretching and bending vibrations.

3.6 Photocatalytic studies

3.6.1 Effect of pH of solution

In photocatalytic degradation, the pH of the sample solution is very important because it influences the degradation efficiency and states about the surface charge properties of the photocatalyst. To study the effect of pH solution was carried out in the range of pH 2–10 at a constant initial concentration of MB and CPS (10 mg/L) with catalyst dose 0.1 gm/L. The zero point of charge (pH_{ZPC}) of α-Bi_2O_3 is 6.3 which indicates that at $pH < pH_{ZPC}$ catalyst surface is positively charged while at $pH > pH_{ZPC}$ negatively charged respectively. In the case of MB dye, it shows the maximum degradation at pH 2 although it is a cationic dye. At pH 2 catalyst surface is positively charged, and the redox potential of the photogenerated valence band holes is sufficiently positive to generate hydroxyl radicals. Also, the positive hole plays vital role to trap the MB molecule and leads to the direct oxidation of MB dye and degrade up to 72% in 60 min Fig. 7. [28].

For the CPS, the Pk_a value is 4.6 therefore, at pH the $pH < Pk_a$ value positively charged protonated CPS predominates, while at $pH > Pk_a$ value negatively charged CPS anions predominates. Hence shows the maximum degradation at pH 5 i.e. greater than the Pk_a of CPS. At this pH the positively charged surface of photocatalyst electrostatically attracts the negatively charge CPS anions and leads to the maximum degradation up to 67% in 60 min Fig. 7. [29].

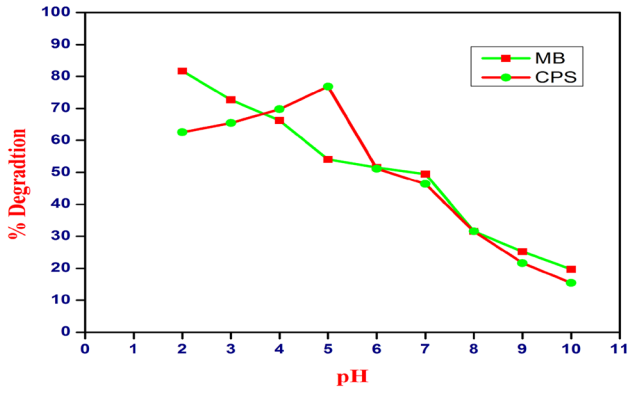

Fig. 7 Effect of pH on photocatalytic degradation of MB and CPS, at, conditions: pH = 2–10, dye concentration 10 mg/L and catalyst dose 0.1 gm/L for the irradiation time 60 min

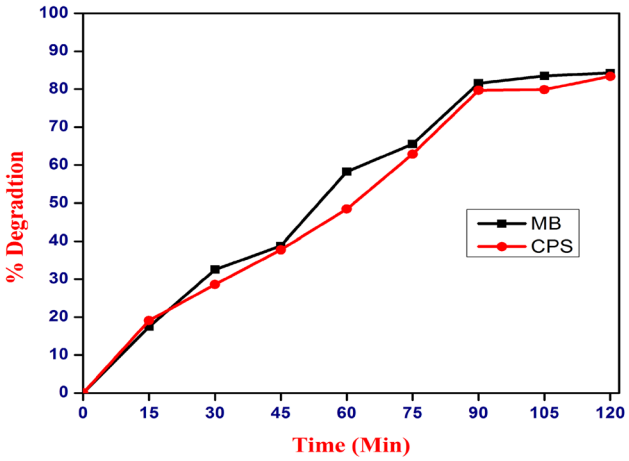

Fig. 9 Effect of irradiation time on photocatalytic degradation of MB, conditions pH = 10, dye concentration 10 mg/L and catalyst dose 0.1 gm/L irradiation time 120 min. and for CPS conditions: pH = 5 CPS concentration 10 mg/L and catalyst dose 0.1 gm/L irradiation time 120 min

3.6.2 Effect of initial concentration

The influence of initial concentration of MB and CPS on degradation efficiency of α-Bi_2O_3 NPs were studied by varying the initial concentration of MB and CPS from 10 to 20 mg/L at optimized pH of both and the catalyst doses 0.1 gm/L for 60 min. The results are as shown in Fig. 8a, b, the photocatalytic degradation efficiency of α-Bi_2O_3 NPS are decreasing with an increase in the initial concentration of MB and CPS solution from 10 mg/L to 20 mg/L. The photocatalytic degradation is completely depends on the generation of hydroxyl radicals and positive holes. But as the initial concentration of MB and CPS increases, the generated of hydroxyl radicals and positive holes will be reduced. Hence the degradation efficiency of α-Bi_2O_3 NPs is decreasing as the initial concentration of MB and CPS increases [30].

3.6.3 Effect of irradiation time

The effect of irradiation time on the photocatalytic efficiency of the catalyst was examined by keeping the other parameter constant. The results are as shown in Fig. 9. It indicates that the photocatalytic efficiency of the catalyst increase with irradiation time up to 90 min. As seen in Fig. 8. When the irradiation time was longer than 90 min, the photocatalytic efficiency is not increased. Because large numbers of small molecules are generated by the photocatalytic degradation process as the irradiation time too long and these small molecules were adsorbed on the catalyst surface, results in the decreased in the formation of hydroxyl radical that degrade the MB and CPS. Hence the increase in the irradiation time does not lead to the maximum degradation [31].

3.6.4 Effect of catalyst dose

The effect of photocatalyst dose was studied at the optimized condition of MB and a CPS by varying the catalyst dose from 0.2 to 1.0 gm/L. The results are as shown in Fig. 10. It shows that the photocatalytic efficiency were increased with catalyst dose for both MB and CPS, this is

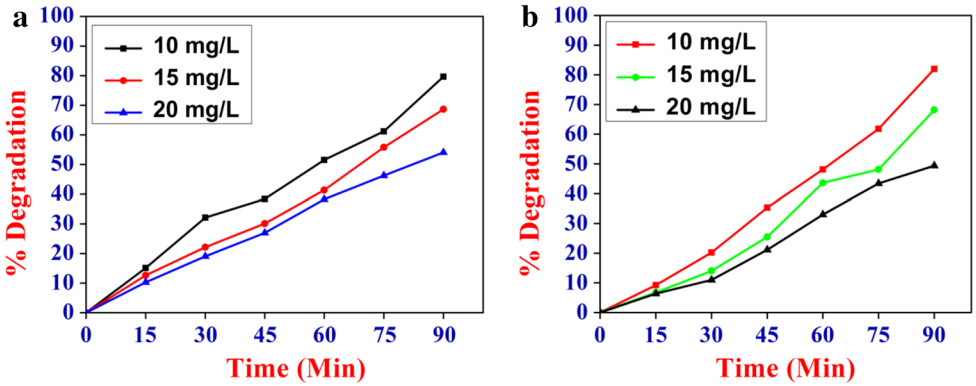

Fig. 8 Effect of initial dye concentration on the photocatalytic degradation **a** MB, conditions pH = 2, dye concentration 10, 15, 20 mg/L and catalyst dose 0.1 gm/L for irradiation time 60 min. **b** CPS, conditions: pH = 5, CPS concentration 10, 15, 20 mg/L and catalyst dose 0.1 gm/L for irradiation time 60 min

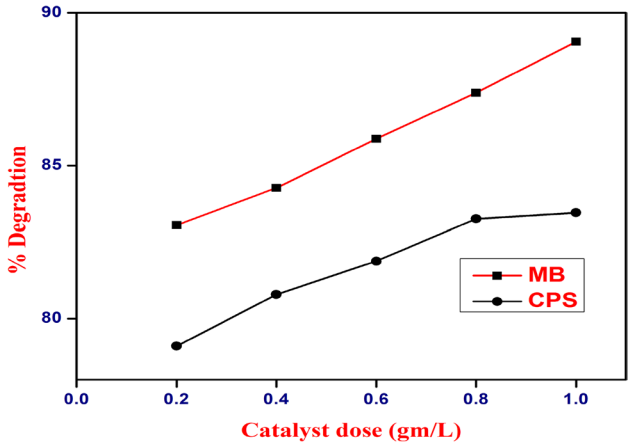

Fig. 10 Effect of catalyst doset on the photocatalytic degradation of MB, conditions pH = 2, dye concentration 10 mg/L and catalyst dose 0.2–1 gm/L irradiation time 90 min. CPS, conditions: pH = 5 CPS concentration 10 mg/L and catalyst dose 0.2–1 gm/L irradiation time 90 min

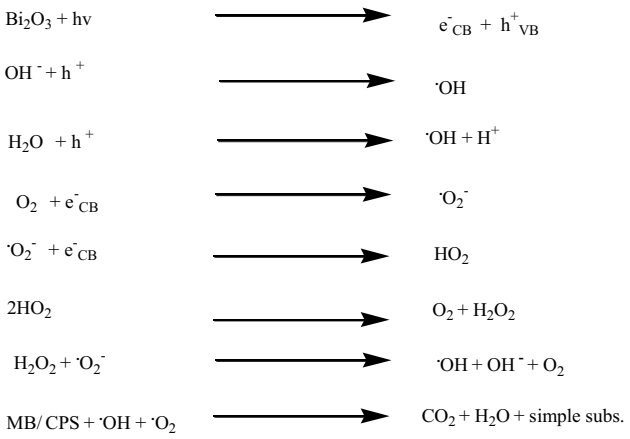

Scheme 1 Mechanism of photocatalytic degradation of MB and CPS

because of as we know that the photocatalytic efficiency completely based on the hydroxyl radical and positive hole generation. Therefore, as the catalyst dose increases the surface area also increases, which leads to the greater number of hydroxyl radical and positive holes were generated. Hence the photocatalytic efficiency, enhanced as the catalyst dose increased [32]. Based on the above study the possible mechanism for the photocatalytic degradation of MB and CPS can be explained by the Scheme 1.

3.6.5 Kinetics study

3.6.5.1 Pseudo first order kinetics To study the kinetics of photocatalytic degradation of the MB and CPS in aqueous suspension, the experiment was performed at the optimized condition of both MB and CPS. The photocatalytic degradation of both follows the pseudo first order kinetics Fig. 11a, b. The pseudo first order kinetics can be represented as shown in Eq. 3. [33].

$$\ln \frac{C_0}{C_t} = kt \tag{3}$$

where k is rate constant, C_0 is the initial concentration and C_t is the concentration at time t. From Fig. 11a, b, it is clearly seen that the ln C_0/C_t is directly proportional to the irradiation time. The rate constant k was determined from the slope of the straight line. The rate constant for MB is 0.01842 and 0.02993 min^{-1} respectively, and having a good correlation with linear regression coefficient (R^2).

4 Conclusion

In the present study, α-Bi_2O_3 NPs were successfully synthesized by sol–gel method and characterized by XRD, SEM, TEM, EDX and FTIR techniques. The results of XRD, SEM and TEM confirmed that the α-Bi_2O_3 NPs are present in

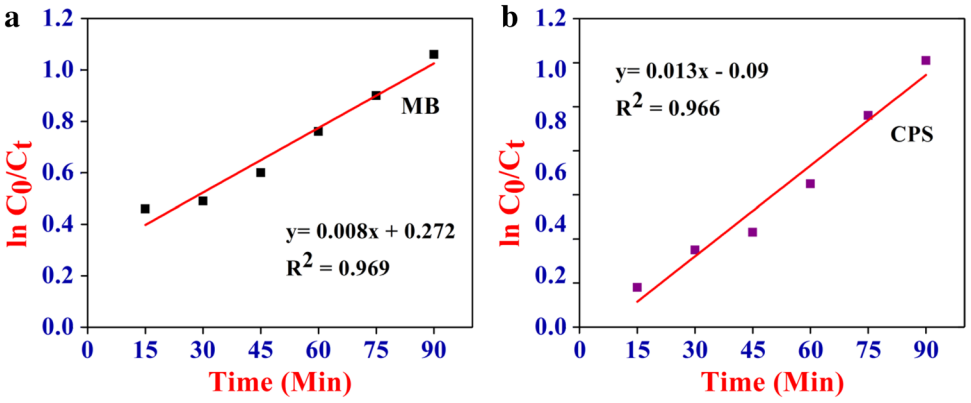

Fig. 11 Pseudo first order kinetics for photocatalytic degradation of **a** MB, conditions pH = 2, dye concentration 10 mg/L and catalyst dose 1 gm/L irradiation time 90 min **b** CPS, conditions: pH = 5 CPS concentration 10 mg/L and catalyst dose 1 gm/L irradiation time 90 min

monoclinic phase with crystalline size below the 1–100 nm and having spherical grains with porous surface morphology. The synthesized α-Bi_2O_3 NPs were utilized as a photocatalyst for the degradation of MB and CPS. To the best of author knowledge, this is the first time report on the photocatalytic degradation of dye and pesticide. The photocatalytic degradation efficiency of photocatalyst increases with the increase in the irradiation time up to 90 min after that it attains the equilibrium. The maximum degradation was obtained with photocatalyst dose 1 mg/L at pH-2 for MB and pH-5 for CPS with 10 mg/L initial concentration of both MB and CPS solution respectively. The photocatalytic degradation of MB and CPS follows the pseudo first kinetics with rate constant is 0.01842 and 0.02993 min^{-1}. Thus the synthesized α-Bi_2O_3 NPs shows the excellent photocatalytic efficiency against the MB dye as compared to the CPS pesticide under UV–visible irradiation.

Acknowledgements The authors gratefully acknowledge to Kaviyitri Bahinabai Chaudhari North Maharashtra University, Jalgaon for providing financial support under the scheme of Shree G. H. Raisoni fellowship for doctoral research and XRD. SEM, EDS and FTIR analysis. Authors are thankful to DST-FIST providing the necessary Grant for instruments. Also, authors are thankful to UGC-DAE-Consortium for Scientific Research, Indore for the TEM analysis.

Compliance with ethical standards

Conflict of interest On behalf of all authors, the corresponding author states that there is no conflict of interest.

References

1. Kamel A, Byrne C, Vigo C, Ferrario J, Stafford C, Verdin G, Siegelman F, Knizner S, Hetrick J (2009) Oxidation of selected organophosphate pesticides during chlorination of simulated drinking water. Water Res 43(2):522–534. https://doi.org/10.1016/j.watres.2008.10.038
2. Bootharaju MS, Pradeep T (2012) Understanding the degradation pathway of the pesticide, chlorpyrifos by noble metal nanoparticles. Langmuir 28(5):2671–2679. https://doi.org/10.1021/la2050515
3. Racke KD (1993) Environmental fate of chlorpyrifos. In: Ware GW (ed) Reviews of environmental contamination and toxicology. Springer, New York, pp 1–150
4. Devi LG, Murthy BN, Kumar SG (2009) Photocatalytic activity of V^{5+}, Mo^{6+} and Th^{4+} doped polycrystalline TiO_2 for the degradation of chlorpyrifos under UV/solar light. J Mol Catal A Chem 308(1):174–181. https://doi.org/10.1016/j.molcata.2009.04.007
5. Hossain MS, Fakhruddin ANM, Chowdhury MAZ, Alam MK (2013) Degradation of chlorpyrifos, an organophosphorus insecticide in aqueous solution with gamma irradiation and natural sunlight. J Environ Chem Eng 1(3):270–274. https://doi.org/10.1016/j.jece.2013.05.006
6. Warner CL, Addleman RS, Cinson AD, Droubay TC, Engelhard MH, Nash MA, Yantasee W, Warner MG (2010) High-performance, superparamagnetic, nanoparticle-based heavy metal sorbents for removal of contaminants from natural waters. Chem Sus Chem 3(6):749–757. https://doi.org/10.1002/cssc.201000027
7. Campelo JM, Luna D, Luque R, Marinas JM, Romero AA (2009) Sustainable preparation of supported metal nanoparticles and their applications in catalysis. Chem Sus Chem 2(1):18–45. https://doi.org/10.1002/cssc.200800227
8. Chong MN, Jin B, Chow CWK, Saint C (2010) Recent developments in photocatalytic water treatment technology: a review. Water Res 44(10):2997–3027. https://doi.org/10.1016/j.watres.2010.02.039
9. Gomez S, Marchena CL, Pizzio L, Pierella L (2013) Preparation and characterization of TiO_2/HZSM-11 zeolite for photodegradation of dichlorvos in aqueous solution. J Hazard Mater 258–259:19–26. https://doi.org/10.1016/j.jhazmat.2013.04.030
10. Gaya UI, Abdullah AH (2008) Heterogeneous photocatalytic degradation of organic contaminants over titanium dioxide: a review of fundamentals, progress and problems. J Photochem Photobiol C 9(1):1–12. https://doi.org/10.1016/j.jphotochemrev.2007.12.003
11. Shifu C, Gengyu C (2005) Photocatalytic degradation of organophosphorus pesticides using floating photocatalyst TiO_2·SiO_2/beads by sunlight. Sol Energy 79(1):1–9. https://doi.org/10.1016/j.solener.2004.10.006
12. Wei L, Shifu C, Wei Z, Sujuan Z (2009) Titanium dioxide mediated photocatalytic degradation of methamidophos in aqueous phase. J Hazard Mater 164(1):154–160. https://doi.org/10.1016/j.jhazmat.2008.07.140
13. Avasarala BK, Tirukkovalluri SR, Bojja S (2011) Photocatalytic degradation of monocrotophos pesticide—an endocrine disruptor by magnesium doped titania. J Hazard Mater 186(2):1234–1240. https://doi.org/10.1016/j.jhazmat.2010.11.132
14. Chen S, Liu Y (2007) Study on the photocatalytic degradation of glyphosate by TiO_2 photocatalyst. Chemosphere 67(5):1010–1017. https://doi.org/10.1016/j.chemosphere.2006.10.054
15. Leontie L, Caraman M, Alexe M, Harnagea C (2002) Structural and optical characteristics of bismuth oxide thin films. Surf Sci 507–510:480–485. https://doi.org/10.1016/S0039-6028(02)01289-X
16. Fan HT, Teng XM, Pan SS, Ye C, Li GH, Zhang LD (2005) Optical properties of δ-Bi_2O_3 thin films grown by reactive sputtering. Appl Phys Lett 87(23):231916. https://doi.org/10.1063/1.2136351
17. Deng H-Y, Hao W-C, Xu H-Z (2011) A transition phase in the transformation from α-, β- and ϵ- to δ-bismuth oxide. Chin Phys Lett 28(5):056101. https://doi.org/10.1088/0256-307x/28/5/056101
18. Salazar-Pérez A, Camacho-López M, Morales-Luckie R, Sánchez-Mendieta V, Ureña-Núñez F, Arenas-Alatorre J (2005) Structural evolution of Bi_2O_3 prepared by thermal oxidation of bismuth nano-particles. Superf Vacío 18(3):4–8
19. Fan H, Pan S, Teng X, Ye C, Li G, Zhang L (2006) δ-Bi_2O_3 thin films prepared by reactive sputtering: fabrication and characterization. Thin Solid Films 513(1–2):142–147
20. Bian Z, Zhu J, Wang S, Cao Y, Qian X, Li H (2008) Self-assembly of active Bi_2O_3/TiO_2 visible photocatalyst with ordered mesoporous structure and highly crystallized anatase. J Phys Chem C 112(16):6258–6262
21. Nezamzadeh-Ejhieh A, Hushmandrad S (2010) Solar photodecolorization of methylene blue by CuO/X zeolite as a heterogeneous catalyst. Appl Catal A 388(1):149–159. https://doi.org/10.1016/j.apcata.2010.08.042
22. Buthiyappan A, Aziz ARA, Daud WMAW (2016) Recent advances and prospects of catalytic advanced oxidation process in treating textile effluents. Rev Chem Eng 32(1):1–47
23. Khairnar SD, Patil MR, Shrivastava VS (2018) Hydrothermally synthesized nanocrystalline Nb_2O_5 and its visible light

photocatalytic activity for the degradation of Congo-red and methylene blue. Iran J Catal 8(2):143–150
24. Yang X, Lian X, Liu S, Wang G, Jiang C, Tian J, Chen J, Wang R (2012) Enhanced photocatalytic performance: a β-Bi_2O_3 thin film by nanoporous surface. J Phys D Appl Phys 46(3):035103
25. Aroutiounian V, Arakelyan V, Shahnazaryan G (2005) Metal oxide photoelectrodes for hydrogen generation using solar radiation-driven water splitting. Sol Energy 78(5):581–592
26. Viruthagiri G, Kannan P, Shanmugam N (2018) Photocatalytic rendition of Zn^{2+}-doped Bi_2O_3 nanoparticles. Photon Nanostruct 32:35–41
27. Jha RK, Pasricha R, Ravi V (2005) Synthesis of bismuth oxide nanoparticles using bismuth nitrate and urea. Ceram Int 31(3):495–497. https://doi.org/10.1016/j.ceramint.2004.06.013
28. Amalraj A, Pius A (2015) Photocatalytic degradation of monocrotophos and chlorpyrifos in aqueous solution using TiO_2 under UV radiation. J Water Process Eng 7:94–101. https://doi.org/10.1016/j.jwpe.2015.06.002
29. Verma A, Dixit PD (2012) Photocatalytic degradability of insecticide Chlorpyrifos over UV irradiated titanium dioxide in aqueous phase. Int J Environ Sci 3:743–755
30. Shankar MV, Cheralathan KK, Arabindoo B, Palanichamy M, Murugesan V (2004) Enhanced photocatalytic activity for the destruction of monocrotophos pesticide by TiO_2/Hβ. J Mol Catal A Chem 223(1):195–200. https://doi.org/10.1016/j.molcata.2004.03.059
31. Wei L, Shifu C, Wei Z, Sujuan Z (2009) Titanium dioxide mediated photocatalytic degradation of methamidophos in aqueous phase. J Hazard Mater 164(1):154–160. https://doi.org/10.1016/j.jhazmat.2008.07.140
32. Muhamad SG (2010) Kinetic studies of catalytic photodegradation of chlorpyrifos insecticide in various natural waters. Arab J Chem 3(2):127–133. https://doi.org/10.1016/j.arabjc.2010.02.009
33. Patil MR, Khairnar SD, Shrivastava VS (2016) Synthesis, characterisation of polyaniline–Fe_3O_4 magnetic nanocomposite and its application for removal of an acid violet 19 dye. Appl Nanosci 6(4):495–502. https://doi.org/10.1007/s13204-015-0465-z